Theoretical Investigation on the Mechanism of the CuI-Catalyzed Carbon−Nitrogen Coupling Reaction of 2-Iodo-selenophene with Benzamide

Pei-yi Wang,[†,‡] Lai-cai Li,[*,†] Chun Yang,[‡] and Yan-rong Li[§]

Department of Chemistry and Key Laboratory of Computer Software, Sichuan Normal University, Chengdu 610068, China, and School of Microelectronics Engineering, University of Electronics Science and Technology, Chengdu 610054, China

Received: June 26, 2007; In Final Form: October 25, 2007

The mechanism of the carbon−nitrogen coupling reaction of 2-iodo-selenophene with benzamide catalyzed by CuI has been investigated with density functional theory at the GGA/PW91/DND and GGA/PBE/DNP levels. The geometric configurations of the reactants, intermediates, transition states, and products were optimized and verified by means of vibration frequency calculations. A four-step mechanism was proposed for the reaction. The first step was the rate-control step. Two possible pathways in the fourth step were investigated, and the main pathway was identified by comparing their activation and dissociation energies. For comparison, the same calculations were performed to the reaction without the CuI activator. The activation barrier with CuI is 76 kJ mol^{-1} smaller than that without CuI. It turns out that CuI can promote the reaction by lowering the activation energy. Our calculations reveal the crucial role of CuI in the reaction and agree well with experimental findings.

1. Introduction

The carbon−nitrogen coupling reaction has become attractive in chemistry in recent years, often used to synthesize some complexes from simple molecules.[1−3] It also takes up a vital place in the pharmaceutical industry.[4] Therefore, developing new methodologies for this reaction and understanding their reaction mechanisms are of great interest in modern theoretical and synthetic chemistry.

The carbon−heteroatom bond formation catalyzed by transition metals has been the subject of many studies during the past few years.[5−7] Although a number of conventional methods exist for carbon−nitrogen bond construction,[8−14] they typically undergo some problems, such as harsh conditions, expensive reagents, and numerous synthetic steps. Even though some recent progress in palladium-catalyzed reactions has partially solved the problems,[15−18] copper catalysts still hold the advantage of low cost for large-scale industrial applications.

Soares do Rêgo Barros[19] et al. have found that 2-iodo-selenophene can be effectively applied to the preparation of carbon−nitrogen bond formation by using CuI as a catalyst and an aliphatic diamine, which is inexpensive, as a ligand (Scheme 1). The reaction proceeds at a lower temperature and milder conditions than the conventional approaches. This was considered as a great breakthrough in the field. However, the mechanism of these reactions still remains unclear. To make a better understanding to these reactions, we investigated the typical reaction of 2-iodo-selenophene with benzamide using density functional theory (DFT). The computational details are described in next section. In section 3, we present the calculated results and discuss the reaction mechanism. The NMR calculations for the product are given in section 4, followed by a conclusion in section 5.

SCHEME 1

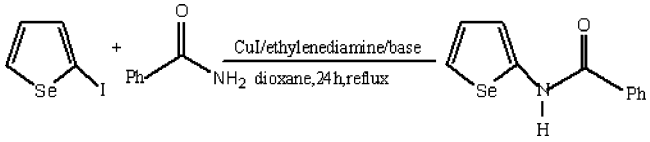

2. Computational Details

All calculations have been performed using DMol[3] code[20−22] as implemented in Accelrys Materials Studio 4.0. The generalized gradient approximation (GGA) with the Perdew−Wang (PW91)[23] exchange−correlation functional is selected in the DFT calculations. Effective core potentials (ECPs) have been employed for the all-electron calculation, where the effect of core electrons is substituted by a simple potential including some degree of relativistic effects. This technique is computationally inexpensive and a good approximation for elements with atomic numbers more than 21. The convergence criteria for geometry optimization were 2×10^{-5} hartree, 0.004 hartree/Å, 0.005 Å, and 1×10^{-5} hartree for energy, force, displacement, and self-consistent field (SCF) density, respectively. DMol[3] utilizes a basis set of numeric atomic functions, which are exact solutions to the Kohn−Sham equations for the atom.[24] The basis set of double numerical plus d-functions (DND) was used throughout the study.

To improve the calculational precision and compare another method with PW91, all geometries have been optimized by GGA/Perdew, Burke, and Enzerhof (PBE)/double numerical plus polarization (DNP).The other computational parameter is not changed. The following discussion is according to the results of GGA/PBE/DNP.

Preliminary transition-state geometries are obtained using the integrated linear synchronous transit/quadratic synchronous

* Author to whom correspondence should be addressed. E-mail: liline33@sohu.com.
† Department of Chemistry, Sichuan Normal University.
‡ Key Laboratory of Computer Software, Sichuan Normal University.
§ University of Electronics Science and Technology.

10.1021/jp074968u CCC: $40.75
Published on Web 01/01/2008

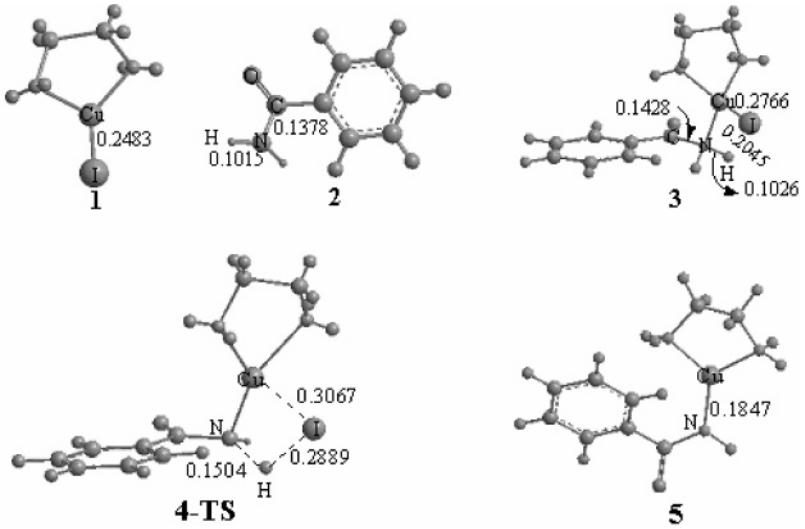

Figure 1. Geometries and partial bond lengths (nm) in the first step of the reaction.

SCHEME 2

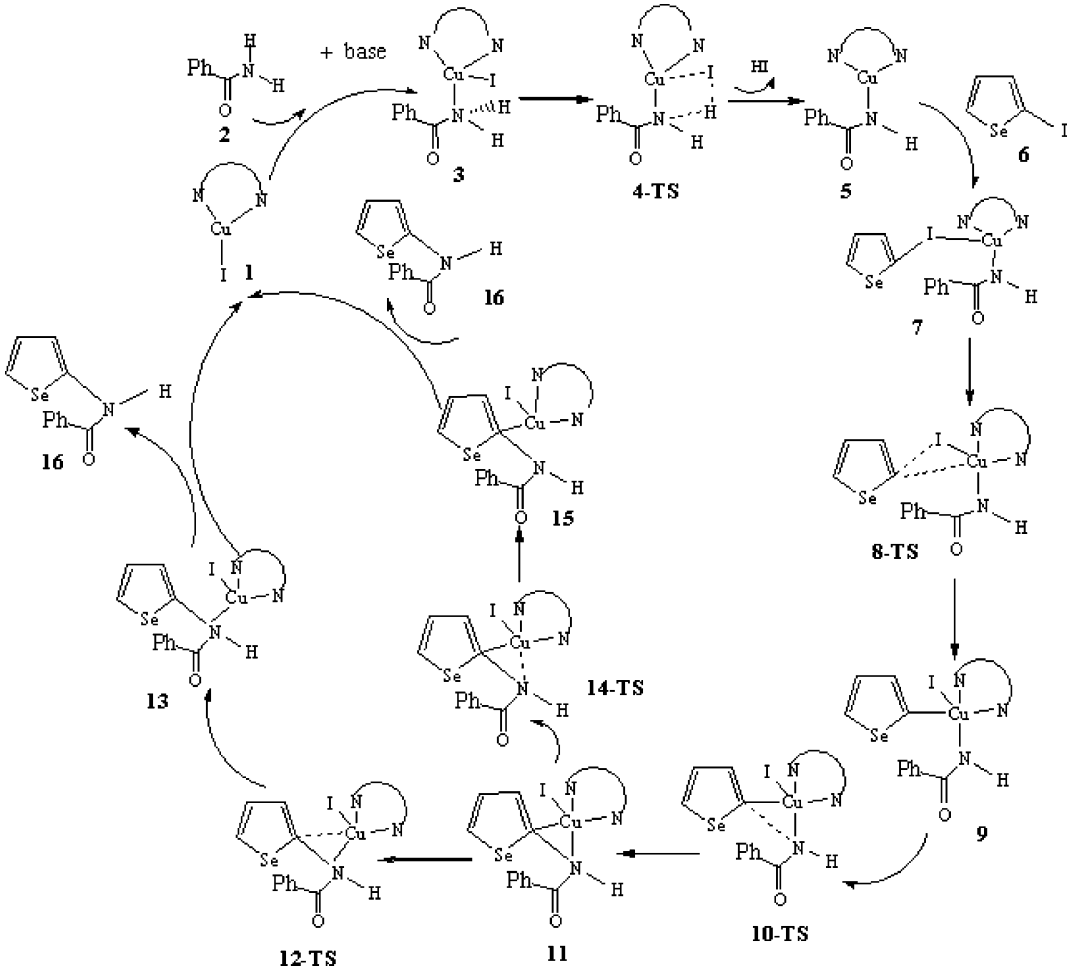

transit (LST/QST) method.[25] All structures identified as stationary points are subject to full-frequency analysis to verify their classification as equilibrium geometries (zero imaginary frequencies) or transition states (one imaginary frequency).

3. Results and Discussion

In this work, as shown in Scheme 2, we have explored the catalytic cycle for the reaction of 2-iodo-selenophene and benzamide. The corresponding geometries are listed in Figures 1−4, respectively.

3.1. Process of the Reaction with CuI Activator. Our calculations indicate that the whole reaction in the presence of CuI consists of four steps during which five transition states are formed. Figures 1−4 give the geometries of the reactants, intermediates, transition states, and products.

*3.1.1. First Step—Formation of Intermediate **5**.* The Cu atom in **1** is attacked by the N atom in **2**, leading to the formation of complex **3**. In this process, the bond length of Cu−I is 0.2483 nm in **1**, while it becomes 0.2766 nm in **3**, 0.0283 nm longer

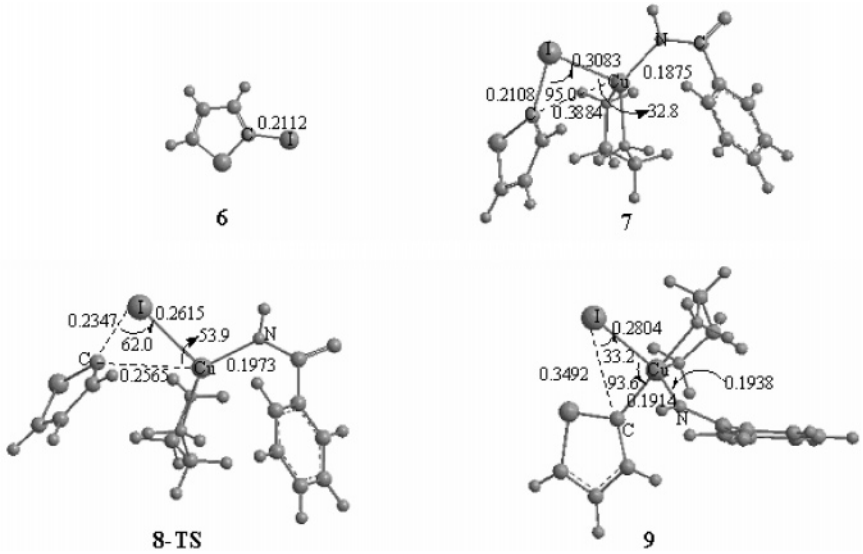

Figure 2. Geometries, partial bond lengths (nm), and angles (deg) in the second step of the reaction.

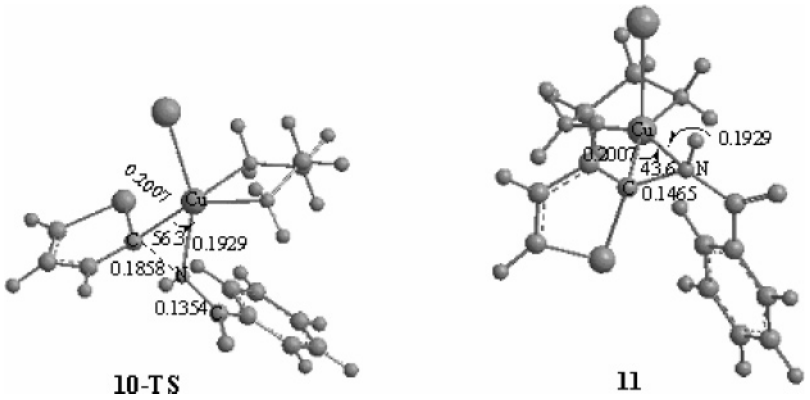

Figure 3. Geometries, partial bond lengths (nm), and angles (deg) in the third step of the reaction.

than that in **1**. In addition, the bond length of C−N is 0.1378 nm in **2**, while it is 0.1428 nm in **3**, 0.0050 nm longer than that in **2**. Therefore, the formation of the N−Cu bond weakens distinctly the Cu−I and C−N bonds. The corresponding stabilization energy is 47 kJ mol^{-1}, as shown in Table 1. Thus, the formation of complex **3** is favorable in energy.

In complex **3**, the I and H atoms may detach and form HI and **5**. To verify the process, we have located the transition state **4-TS**, a four-membered ring. For the **4-TS** structure, the only imaginary frequency is 1230.2 cm^{-1}. Analysis of the vibration modes indicates that this imaginary frequency is associated with Cu−I, N−H, and H−I stretching motions. The bond lengths of Cu−I and N−H increase, while the bond length of H−I decreases at the same time. The bond lengths of Cu−I, N−H, and H−I are 0.2766, 0.1026, and 0.3148 nm in complex **3** but 0.3067, 0.1504, and 0.2889 nm in **4-TS,** respectively. The bond lengths of Cu−I and N−H increase by 0.0301 and 0.0478 nm respectively, while the bond length of H−I decreases by 0.0259 nm. Obviously, the Cu−I and N−H bonds are partly broken, and the H−I bond is partly formed in **4-TS**.

After the reaction surpasses the transition state **4-TS**, I and H atoms detach, and intermediate **5** is formed. The activation energy, listed in Table 1, is 185 kJ mol^{-1} for the reaction from complex **3** to **4-TS**, which is high comparatively. So it is the rate-controlling step of the reaction.

3.1.2. Second Step—Formation of Intermediate 9. In configuration **6**, the I atom is electrophilic and tends to attack the Cu atom in **5** to form complex **7**. The bond length of N−Cu increases from 0.1847 nm in **5** to 0.1875 nm in complex **7**, indicating that the N−Cu bond is weakened in the formation of the I−Cu bond in **7**. The corresponding stabilization energy is 2 kJ mol^{-1}.

In complex **7**, it is possible that the C atom attacks the Cu atom, and the C−I bond breaks. A transition state, **8-TS,** with a three-membered ring, was found in the confirmation of the process. **8-TS** possesses an imaginary frequency of 137.9 cm^{-1}. Vibration mode analysis reveals that this imaginary frequency is associated with C−I and C−Cu bond stretching motions. The bond lengths of C−I and C−Cu are 0.2108 and 0.3884 nm in complex **7** but 0.2347 and 0.2565 nm in **8-TS**, respectively. The C−I bond increases by 0.0239 nm, and the C−Cu bond decreases by 0.1319 nm. It is clear that the C−I bond is partly broken and the C−Cu bond is partly formed in **8-TS** at the same time. This is a concerted process.

After the reaction surpasses the transition state **8-TS**, intermediate **9** is formed. The bond lengths of C−I and C−Cu in **9** are 0.3492 and 0.1914 nm, respectively. Our results show that the C−I bond is completely broken and the C−Cu is completely formed in **9**. In addition, the C−Cu−I angles are 32.8°, 53.9°, and 93.6° in complex **7**, transition state **8-TS**, and intermediate **9,** respectively, while the corresponding C−I−Cu angles are 95.0°, 62.0°, and 33.2° in the three states. Considering the direction of angle change, one can see that complex **7** is transformation intermediate **9** through **8-TS**. The activation energy of this process is 42 kJ mol^{-1}, which is favorable for the reaction to proceed.

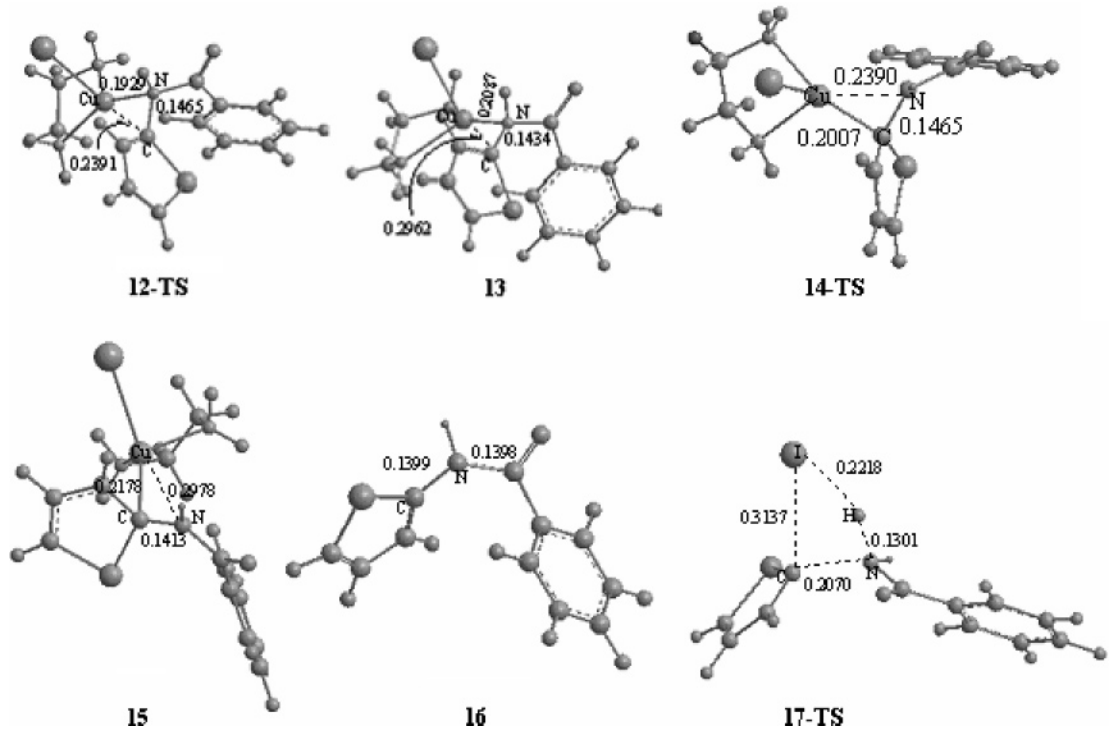

Figure 4. Geometries, partial bond lengths (nm), and angles (deg) in the fourth step of the reaction.

TABLE 1: Energies (a.u.) and Relative Energies (kJ mol^{-1}) and Frequencies (cm^{-1}) of the Compounds in the Reaction

species	*E* (GGA/PW91/DND)	E_{rel}	*E* (GGA/PBE/DNP)	E_{rel}	frequencies
1 + **2**	−800.446779	0	−799.898663	0	
3	−800.484949	−100.22	−799.916693	−47.34	
4-TS	−800.412990	88.71	−799.846206	137.74	1230.2i
5 + HI	−800.413663	86.95	−799.854357	116.33	
5 + **6**	−963.376804	0	−962.682757	0	
7	−963.377615	−2.13	−962.683346	−1.55	
8-TS	−963.368724	21.21	−962.667807	40.80	137.9i
9	−963.399516	−59.63	−962.700761	−47.27	
10-TS	−963.376365	1.15	−962.669079	35.91	300.9i
11	−963.418529	−109.55	−962.713021	−79.46	
12-TS	−963.416488	−104.19	−962.712024	−76.85	61.9i
13	−963.431999	−144.91	−962.728400	−119.84	
14-TS	−963.384674	−20.66	−962.707668	−65.40	85.5i
15	−963.449863	−191.82	−962.740429	−151.42	
16 + **1**	−963.417566	−107.02	−962.724388	−109.30	
6 + **2**	−575.917810	0	−575.466852	0	
17-TS	−575.837848	209.94	−575.367293	261.39	1130.9i
16 + HI	−575.925439	−20.03	−575.464177	7.02	

*3.1.3. Third Step—Formation of Intermediate **11**.* In intermediate **9**, the C atom attacks the N atom and forms configuration **11,** a three-membered ring. A transition state, **10-TS**, is located in the process. **10-TS** is a three-membered ring with one imaginary frequency of 300.9 cm^{-1}. Analysis of the vibration modes indicates that this imaginary frequency is associated with the C−N bond stretching motion. The C−N bond varies from 0.2754 nm in **9** to 0.1858 nm in **10-TS.** Clearly, the C−N bond is partly formed in **10-TS**.

After the reaction surpasses **10-TS**, the intermediate **11** is formed. The C−N bond length in **11** is 0.1465 nm, 0.0393 nm shorter than that in **10-TS**. It turns out that the C−N bond is completely formed in **11**. In addition, the C−Cu−N angles are 91.3°, 56.3°, and 43.6° in **9**, **10-TS**, and **11,** respectively. Indicated by the decreasing C−Cu−N angle in the process, we can see that intermediate **9** is transformed into intermediate **11** through transition state **10-TS**. The corresponding activation energy is 83kJ mol^{-1}.

*3.1.4. Fourth Step—Formation of Product **16**.* Intermediate **11** is unstable. The C−Cu and N−Cu bonds in **11** can break easily. Two possible bond breaking modes that lead to two different reaction pathways to form product **16** were proposed and examined in this study. The two reaction pathways are discussed as follows:

In the first pathway, the C−Cu bond breaks and forms a transition state of **12-TS**. Analysis of the vibration modes shows that the imaginary frequency (61.9 cm^{-1}) in **12** is associated with the C−Cu bond stretching motion. The bond length of C−Cu is 0.2391 nm, 0.0284 nm longer than that in **11**. It turns out that the C−Cu bond is partly broken in **12-TS**.

After the reaction surpasses **12-TS**, intermediate **13** is formed. The bond length of C−Cu is 0.2962 nm, which is 0.0571 nm longer than that in **12-TS**. It is clear that the C−Cu bond is completely broken in **13**. In addition, the C−N−Cu angles are 71.0°, 88.5°, and 113.2° in **11**, **12-TS**, and **13**, respectively. With the C−N−Cu angle changes, **11** transforms into **13** through

TABLE 2: Chemical Shifts and Relative Errors of the Product

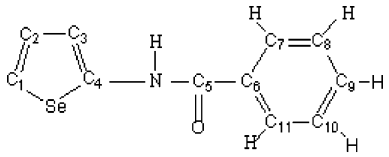

product **16**

atoms	C1	C2	C3	C4	C5	C6	C7	C8	C9	C10	C11
calculated	133.4	118.3	116.7	152.2	159.7	126.5	124.6	120.8	124.1	120.8	124.6
observed [19]	132.9	123.7	112.6	141.6	163.6	132.2	128.9	126.0	127.1	126.0	128.9
relative errors	0.34%	4.37%	3.64%	7.52%	2.38%	4.33%	3.35%	4.15%	2.35%	4.15%	3.35%

transition state **12-TS**. As shown in Table 1, the corresponding activation energy is 3 kJ mol^{-1}, a small barrier favorable to the reaction.

CuI can detach from intermediate **13** with a dissociation energy of 11 kJ mol^{-1}. Both product **16** and activator **1** are formed in the process. The formed CuI may combine with reactant **2** and start the next cycle of the reaction. Therefore CuI serves as a catalyst, promoting the reaction to give a high yield, which is in good agreement with the experimental result.[19]

In the second pathway, the N−Cu bond breaks and forms a transition state of **14-TS**, which directly connects **11** with **15** and has one imaginary frequency of 85.5 cm^{-1}. Analysis of the vibration modes shows that this imaginary frequency is associated with the N−Cu bond stretching motion. The bond length of N−Cu is 0.2390 nm in **14-TS**, 0.0461 nm longer than that in **11**. It turns out that the N−Cu bond is partly broken in **14-TS**.

After the reaction surpasses **14-TS**, intermediate **15** is formed. The bond length of N−Cu is 0.2978 nm in **15**, 0.0588 nm longer than that in **14-TS**. The activation energy of the step is 14 kJ mol^{-1}. CuI can also detach from **15** with a dissociation energy of 42 kJ mol^{-1}. Both product **16** and activator **1** are formed in the process. The formed CuI then starts the next cycle of the reaction with reactant **2.**

The activation energy of the second pathway is 12 kJ mol^{-1} higher than that in the first pathway. Moreover, the dissociation energy of the second pathway is 32 kJ mol^{-1} greater than that in the first pathway. The first pathway is therefore the main pathway in the reaction.

3.2. Reaction Process without CuI Activator. To illuminate the activation effect of CuI, we studied further the reaction without CuI. In the process of configuration **6** reacting with **2** to form product **16** and HI in the absence of CuI, we found transition state **17-TS,** a four-membered ring with one imaginary frequency at 1130.9 cm^{-1}. Analysis of the vibration modes indicates that this imaginary frequency is associated with C−I, I−H, N−H, and C−N bond stretching motions. The bond lengths of C−I and N−H increase, while the bond lengths of I−H and C−N decrease at the same time. The C−I bond length varies from 0.2112 nm in **6** to 0.3137 nm in **17-TS**, while the N−H bond length varies from 0.1015 nm in configuration **2** to 0.1301 nm in **17-TS**. It is clear that the C−I and N−H bonds in **17-TS** are partly broken.

After the reaction surpasses **17-TS**, product **16** and HI are formed. The bond length of C−N decreases from 0.2070 nm in **17-TS** to 0.1399 nm in **16**, indicating that the C−N bond in product **16** is completely formed. As shown in Table 1, the activation energy of the step is 261 kJ mol^{-1}, which is 76 kJ mol^{-1} greater than the highest activation energy in the reaction with CuI activator. One may conclude that the activator CuI can significantly lower the energy barrier and promote the reaction.

From Table 1, we can see that the energy change trend of GGA/PBE/DNP is consistent with that of GGA/PW91/DND.

4. Calculation and Discussion for NMR of the Product

The NMR calculation was carried out with the Gaussian 98[26] program package. The product geometry was optimized with B3LYP at the 6-31G(d) level. Then the NMR of product **16** is calculated with the gauge including atomic orbital (GIAO) method at the same level. Table 2 compares the calculated and measured[19] NMR of product **16.** Our calculations are basically consistent with experiments with relative errors between 0.37% and 7.52%.

5. Conclusions

The microcosmic reaction mechanism of 2-iodo-selenophene and benzamide with CuI activator has been investigated by DFT. A four-step mechanism is proposed for the reaction. The first step to form transition state **4-TS** from complex **3** is the rate-control step with the highest activation energy among all steps. There are two possible reaction pathways; C−Cu or N−Cu breaks to form product **16** from intermediate **11** in the fourth step. The former has lower activation energy and dissociation energy than the latter by 12 and 32 kJ mol^{-1}, respectively, and is thus the main path in the former step. In addition, we have investigated the reaction mechanism in the absence of CuI activator for comparison. Our results show that CuI promotes the reaction by significantly lowering the energy barrier. Our findings reveal the catalytic mechanism of CuI and agree well with the experiments. We also calculated the NMR of product **16.** The calculated results are basically consistent with the experiments.

Acknowledgment. This research work has been supported by the State Key Development Program for Basic Research of China (Grant Nos. 51310Z03 and 61363) and the Science-Technology Foundation for Young Scientists of Sichuan Province, China (Grant No. 07ZQ026-021).We acknowledge the support from the Software Key Laboratory of Sichuan Normal University.

References and Notes

(1) Bartoli, G.; Bosco, M.; Eurico, M.; Petrini, M.; Sambri, L.; Torregiani, E. *J. Org. Chem.* **2001**, *66*, 9052−9055.

(2) Matsubara, S.; Yoshioka, M.; Utimoto, K. *Chem. Lett.* **1994**, *23*, 827−830.

(3) Azizi, N.; Saidi, M. R. *Tetrahedron* **2004**, *60*, 383−387.

(4) Juaristi, E. *Enatioselective Synthesis of β-Amino Acids*; Wiley-VCH: New York, 1997; Chapter 1.

(5) Finet, J. P.; Fedorov, A. V.; Combes, S.; Boyer, G. *Curr. Org. Chem.* **2002**, *6*, 597−626.

(6) Hartwig, J. F. Palladium-catalyzed amination of aryl halides and related reactions. In *Handbook of Organopalladium Chemistry for Organic*

Synthesis; Negishi, E., de Meijere, A., Eds.; Wiley Interscience: New York, 2002; Vol. 1, p 1051.

(7) Muci, A. R.; Buchwald, S. L. *Top. Curr. Chem.* **2002**, *219*, 133.

(8) Lexy, H.; Kauffmann, T. *Chem. Ber.* **1980**, *113*, 2755−2759.

(9) Harbert, C. A.; Plattner, J. J.; Welch, W. M.; Weissman, A.; Koe, B. K. *J. Med. Chem.* **1980**, *23*, 635−643.

(10) Unangst, P. C.; Connor, D. T.; Stabler, S. R.; Weikert, R. J. *J. Heterocycl. Chem.* **1987**, *24*, 811−817.

(11) Kato, Y.; Conn, M. M.; Rebek, J., Jr. *J. Am. Chem. Soc.* **1994**, *116*, 3279−3284.

(12) Murakami, Y.; Watnable, T.; Hagiwara, T.; Akiyama, Y.; Ishii, H. *Chem. Pharm. Bull.* **1995**, *43*, 1281−1286.

(13) Mederski, W. W. K. R.; Lefort, M.; Germann, M.; Kux, D. *Tetrahedron* **1999**, *55*, 12757−127770.

(14) Collman, J. P.; Zhong, M. *Org. Lett.* **2000**, *2*, 1233−1236.

(15) Barluenga, J.; Valdes, C. *Chem. Commun.* **2005**, 4891−4901.

(16) Hartwig, J. F. *Angew. Chem., Int. Ed.* **1998**, *37*, 2046−2067.

(17) Buchwald, S. L.; Yang, B. H. *J. Organomet. Chem.* **1999**, *576*, 125−146.

(18) Hartwig, J. F.; Hamann, B. C.; Shaughnessy, K. H. *J. Org. Chem.* **1998**, *63*, 6546−6553.

(19) Soares do Rego Barros, O.; Nogueira, C. W.; Stangherlin, E. C.; Menezes, P. H.; Zeni, G. *J. Org. Chem.* **2006**, *71*, 1552−1557.

(20) Delley, B. *J. Chem. Phys.* **1990**, *92*, 508−517.

(21) Delley, B. *J. Chem. Phys.* **2000**, *113*, 7756−7764.

(22) Delley, B. *J. Phys. Chem.* **1996**, *100*, 6107−6110.

(23) Perdew, J. P.; Wang, Y. *Phys. Rev. B* **1992**, *45*, 13244−13249.

(24) Delley, B. *Modern Density Functional Theory: A Tool for Chemistry, in: Theoretical and Computational Chemistry, J.M. Seminario, P. Politzer (Eds.),* Elsevier, Amsterdam, 1995, vol. 2.

(25) Halgren, T. A.; Lipscomb, W. N.; *Chem. Phys. Lett.* **1977**, *49*, 225−232.

(26) Frisch, M. J.; Trucks, G. W.; Schlegel, H. B.; Scuseria, G. E.; Robb, M. A.; Cheeseman, J. R.; Zakrzewski, V. G.; Montgomery, J. A., Jr.; Stratmann, R. E.; Burant, J. C.; Dapprich, S.; Millam, J. M.; Daniels, A. D.; Kudin, K. N.; Strain, M. C.; Farkas, O.; Tomasi, J.; Barone, V.; Cossi, M.; Cammi, R.; Mennucci, B.; Pomelli, C.; Adamo, C.; Clifford, S.; Ochterski, J.; Petersson, G. A.; Ayala, P. Y.; Cui, Q.; Morokuma, K.; Malick, D. K.; Rabuck, A. D.; Raghavachari, K.; Foresman, J. B.; Cioslowski, J.; Ortiz, J. V.; Stefanov, B. B.; Liu, G.; Liashenko, A.; Piskorz, P.; Komaromi, I.; Gomperts, R.; Martin, R. L.; Fox, D. J.; Keith, T.; Al-Laham, M. A.; Peng, C. Y.; Nanayakkara, A.; Gonzalez, C.; Challacombe, M.; Gill, P. M. W.; Johnson, B. G.; Chen, W.; Wong, M. W.; Andres, J. L.; Head-Gordon, M.; Replogle, E. S.; Pople, J. A. *Gaussian 98*, revision A.11; Gaussian, Inc.: Pittsburgh, PA, 1998.